Effect of zinc and calcium ions on the rat kidney membrane-bound form of dipeptidyl peptidase IV

Hansel Gómez[1,2], Mae Chappé[1], Pedro A Valiente[1], Tirso Pons[3], María de Los Angeles Chávez[1], Jean-Louis Charli[4] and Isel Pascual[1,*]

[1]*Centro de Estudios de Proteínas (CEP), Facultad de Biología, Universidad de la Habana, Calle 25 No. 455, Vedado, La Habana, 10400, Cuba*

[2]*Departament de Química, Universitat Autònoma de Barcelona, 08193 Bellaterra, Barcelona, Spain*

[3]*Structural Biology and Biocomputing Programme, Spanish National Cancer Research Centre (CNIO), C/Melchor Fernández Almagro 3, Madrid E-28029, Spain*

[4]*Departamento de Genética del Desarrollo y Fisiología Molecular, Instituto de Biotecnología, Universidad Nacional Autónoma de México (UNAM), Cuernavaca, Morelos 62210, México*

**Corresponding author (Fax, 53-7-8321321; Email, isel@fbio.uh.cu; iselpascual@yahoo.es)*

Dipeptidyl peptidase IV (DPP-IV) is an ectopeptidase with many roles, and a target of therapies for different pathologies. Zinc and calcium produce mixed inhibition of porcine DPP-IV activity. To investigate whether these results may be generalized to mammalian DPP-IV orthologues, we purified the intact membrane-bound form from rat kidney. Rat DPP-IV hydrolysed Gly-Pro-*p*-nitroanilide with an average V_{max} of 0.86±0.01 μmol $min^{-1}mL^{-1}$ and K_M of 76±6 μM. The enzyme was inhibited by the DPP-IV family inhibitor L-threo-Ile-thiazolidide (K_i=64.0±0.53 nM), competitively inhibited by bacitracin (K_i=0.16±0.01 mM) and bestatin (K_i=0.23±0.02 mM), and irreversibly inhibited by TLCK (IC_{50} value of 1.20±0.11 mM). The enzyme was also inhibited by divalent ions like Zn^{2+} and Ca^{2+}, for which a mixed inhibition mechanism was observed (K_i values of the competitive component: 0.15±0.01 mM and 50.0±1.05 mM, respectively). According to bioinformatic tools, Ca^{2+} ions preferentially bound to the β-propeller domain of the rat and human enzymes, while Zn^{2+} ions to the α-β hydrolase domain; the binding sites were essentially the same that were previously reported for the porcine DPP-IV. These data suggest that the cationic susceptibility of mammalian DPP-IV orthologues involves conserved mechanisms.

[Gómez H, Chappé M, Valiente P, Pons T, Chávez MLA, Charli J-L and Pascual I 2013 Effect of zinc and calcium ions on the rat kidney membrane-bound form of dipeptidyl peptidase IV. *J. Biosci.* **38** 461–469] **DOI** 10.1007/s12038-013-9333-8

1. Introduction

Dipeptidyl peptidase IV (DPP-IV, EC 3.4.14.5) has attracted intense interest (Matteucci and Giampietro 2009; Peters 2010; Stulc and Sedo 2010). This enzyme is a ubiquitous, homodimeric serine aminopeptidase with broad tissue distribution. DPP-IV preferentially cleaves Xaa-Pro or Xaa-Ala dipeptides from the N-terminus of oligopeptides with approximately 30 or less amino acids. The enzyme processes regulatory peptides *in vivo*, leading to their biological activation or inactivation. It has an important role in multiple physiological functions, such as degradation of glucose-dependent insulinotropic peptide and glucagon-like peptide 1, the most important insulin-releasing hormones of the enteroinsular axis. This enzyme also regulates immune system responses mediated by CD4+ T lymphocytes, and

Keywords. Binding site prediction; cancer; diabetes; dipeptidyl peptidase IV; divalent cations; inhibition

Abbreviations used: aas, amino acids; APA, glutamyl aminopeptidase; APB, arginyl aminopeptidase; APN, alanyl aminopeptidase; BSA, bovine serum albumin; DPP-IV, dipeptidyl peptidase IV; GIP, gastric inhibitory peptide; GLP-1, glucagon-like peptide 1; NEM, *N*-ethyl maleimide; P32/98, L-threo-Ile-thiazolidide; pNA, *p*-nitroanilide; TLCK, tosyl-L-lysine chloromethyl ketone; Xaa, any common amino acids

Published online: 11 July 2013

inactivates endomorphin 2, an analgesic peptide abundant in the cortex of the human brain, with high affinity for the μ-opioid receptors (Gorrell 2005). More recently, high DPP-IV activity has been detected in several pathologies such as hepatic cirrhosis, head-and-neck or prostate cancer, bowel disease, as well as impaired function of the immune system (Gorrell 2005; Bank *et al.* 2008, Wilson *et al.* 2005; Yazbeck *et al.* 2009, Yilmaz *et al.* 2009).

Strategies for inhibition of DPP-IV activity have been developed for the treatment of various diseases, in particular type 2 diabetes mellitus and cancer (Matteucci and Giampietro 2009; Peters 2010; Stulc and Sedo 2010). In several of these pathologies, a deficiency of cations (e.g. zinc) is also implicated (reviewed in Jansen *et al.* 2009). We have recently shown that zinc inhibits the activity of porcine DPP-IV with a K_i value near circulating concentrations in mammals while the effect of calcium was weaker (Pascual *et al.* 2011). To understand whether this sensitivity is a general property of DPP-IV enzymes in mammals, and since rodents are one of the models of choice for many preclinical studies, we purified to homogeneity the intact membrane form of DPP-IV from rat kidney by a method similar to that previously described for the porcine kidney enzyme (Pascual *et al.* 2011). We characterized the effect of divalent cations on enzyme activity, with emphasis on zinc and calcium. To obtain a comparative insight into the interaction between DPP-IV and calcium or zinc ions, their binding sites were predicted in rat and human enzymes and compared to those previously predicted for the porcine orthologue.

2. Materials and methods

2.1 *Materials*

Wistar rat kidneys were kindly donated by the Biology Department, University of Havana, Cuba. DEAE Sephacel and Sephadex G-200 were purchased from Amersham Biosciences; C4 RP-HPLC column from Vydac, bacitracin, tosyl-L-lysine chloromethyl ketone (TLCK), *N*-ethyl maleimide (NEM), EGTA, EDTA, 1,10-phenanthroline, pepstatin, aprotinin and bestatin from Sigma; Gly-Pro-*p*-nitroanilide, Ala-*p*-nitroanilide, Arg-*p*-nitroanilide, Glu-*p*-nitroanilide from Bachem; L-threo-Ile-thiazolidide (P32/98) from Enzo Life Sciences. Other reagents were of analytical grade.

2.2 *Protein determination*

During the purification procedure, the protein concentration was determined at 280 nm using an arbitrary extinction coefficient of 1 (0.1%, 1 cm) in an Ultrospec 4000 spectrometer (Amersham Biosciences) (Scopes 1987). During the enzyme characterization, we used the procedure described by (Scopes 1987) with bovine serum albumin as standard.

2.3 *Determination of DPP-IV and M1 family aminopeptidases activities*

DPP-IV activity was measured at 37°C as described by (Nagatsu *et al.* 1976) using the substrate Gly-Pro-*p*-nitroanilide (Gly-Pro-pNA, 5 mM) in 50 mM Tris-HCl, 0.1% Triton X100, pH 8 buffer [buffer A]. The production of *p*-nitroaniline was measured every 15 s during 3 min at 405 nm, at 37°C, in an Ultrospec 4000 spectrometer. The *p*-nitroaniline extinction coefficient used was 8850 M^{-1} cm^{-1}. One unit of enzymatic activity was defined as the amount of DPP-IV necessary for the hydrolysis of 1 μmol of Gly-Pro-pNA per min in the specified conditions. The assays for alanyl aminopeptidase (APN, EC 3.4.11.2), glutamyl aminopeptidase (APA, EC 3.4.11.7) and arginyl aminopeptidase (APB, EC 3.4.11.6) were designed according to (Tieku and Hooper 1992) using the substrates Ala-pNA, Glu-pNA and Arg-pNA, respectively.

2.4 *Purification of the intact membrane-bound form of rat kidney DPP-IV*

All purification steps were performed at 4°C; a procedure similar to that previously described for porcine kidney cortex DPP-IV was followed (Pascual *et al.* 2011) using the whole organ as starting material.

2.5 *Kinetic analysis*

2.5.1 *Effect of pH on DPP-IV activity and determination of kinetic constants for rat kidney DPP-IV:* Rat kidney DPP-IV concentration was 2×10^{-7} M; the procedure to study the effect of pH on enzyme activity was similar to that described in (Pascual *et al.* 2011). The initial rates were determined with increasing substrate concentrations (Gly-Pro-pNA: 0.015–5.0 mM). The kinetic constants K_M and V_{max} were determined by adjusting the experimental data (n=4) to the Michaelis–Menten curve (Copeland 2000; Chávez *et al.* 1990) using the Grafit program (Leatherbarrow 1993).

2.5.2 *Effect of protease inhibitors on DPP-IV activity:* Inhibitor (0.01–10 mM) effects were determined by quantifying the decrease of DPP-IV activity in aliquots pre-incubated with the inhibitor for 0–60 min at 37°C in buffer A, using 0.07 mM substrate (n=6) (Pascual *et al.* 2011). The IC_{50} value was determined by nonlinear regression analysis of the dose–response curve. For classical competitive inhibition, K_i values were determined as described (Copeland 2000). For the tight

binding inhibitor P32/98 specific for DPP-IV family (Lankas *et al.* 2005), the range of concentration assayed was 0.01–10 μM, and K_i' was determined using the Morrison quadratic equation (Copeland 2000). K_i' was corrected according to $K_i=K_i'/(1+[S]/K_M)$.

2.5.3 *Effect of metal ions on DPP-IV activity:* Rat kidney DPP-IV was pre-incubated at 37°C with the specific salt (0.05–0.5 M; $BaCl_2$, $MnCl_2$, $MgCl_2$, $CdCl_2$, $HgCl_2$, $CaCl_2$, $CoCl_2$ and $ZnCl_2$), for 1 min to attain the equilibrium in buffer A, previously to the addition of 0.07 mM of substrate (n=6). The IC_{50} value was determined by nonlinear regression analysis of the dose–response curve. To study the kinetic mechanisms of inhibition, we followed the general strategy for classical inhibition. We initially investigated the effect of different inhibitor (ion) concentrations on the relation between the initial rate and the substrate concentration. Enzyme assays were performed at increasing substrate concentration (0.015–1.143 mM) in the presence of 10–100 mM $CaCl_2$ or 0.1–1 mM $ZnCl_2$ (n=6). Data were represented as primary Lineweaver–Burk plots ($1/V_o$ vs $1/[S_o]$). This representation allowed us the identification of a mixed type of inhibition for zinc and calcium ions. For the determination of the K_i value, we plotted Lineweaver–Burk slopes vs inhibitor concentrations. These secondary plots were used to determine K_i values, and to identify whether mixed inhibition was total (linear) or partial (hyperbolic) (Cornish-Bowden 2012; Chávez *et al.* 1990).

2.6 *Prediction of Ca^{2+} and Zn^{2+} binding sites in rat and human DPP-IV structures using bioinformatic tools*

The three-dimensional (3D) structure of rat and human DPP-IV extracellular domains, determined by X-ray crystallography, are accessible at Protein Data Bank (*http://www.pdb.org/pdb/*) with accession codes 2gbc (2.8 Å resolution) (Longenecker *et al.* 2006) and 1pfq (1.9 Å resolution) (Oefner *et al.* 2003), respectively. These 3D structures were used to predict the metal binding sites. For the GG program (*http://chemistry.gsu.edu/faculty/Yang/*) (Deng *et al.* 2006), O-O distance parameters were fixed at 6.0 Å, and minimum and maximum distances for Ca^{2+}-O were fixed at 1.8 Å and 3.3 Å, respectively. The default parameters were used with FEATURE and SeqFEATURE programs (*http://feature.stanford.edu/webfeature/*) (Liang *et al.* 2003). Zn^{2+} binding sites were predicted using the MetSite program (*http://bioinf.cs.ucl.ac.uk/MetSite/*) (Sodhi *et al.* 2004) considering a percentage of false positives of 5%. CHIMERA (Pettersen *et al.* 2004) and VMD (Humphrey *et al.* 1996) were used for the graphic representation of Ca^{2+} and Zn^{2+} binding sites. We used

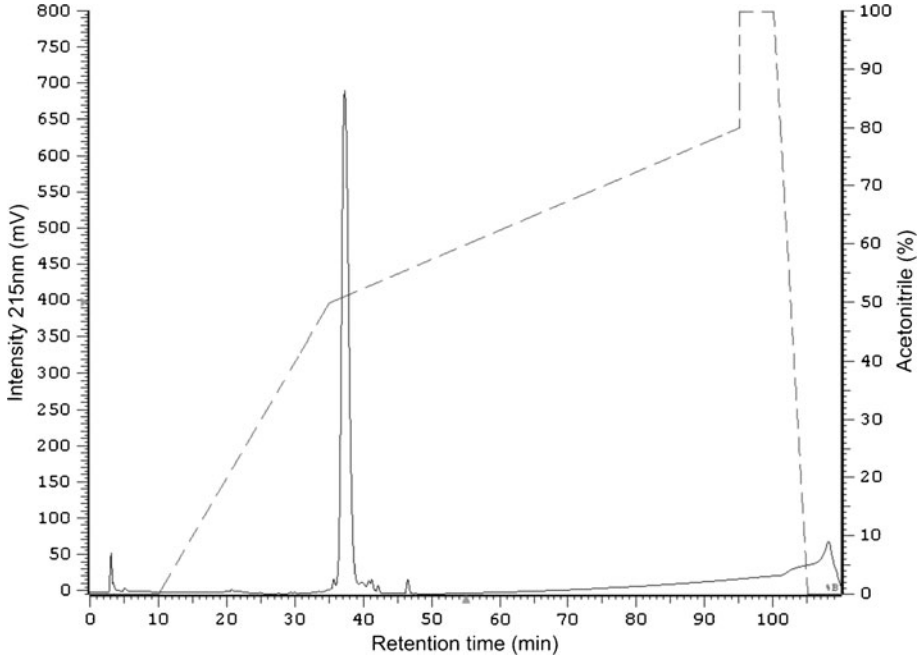

Figure 1. Purity criteria for purified rat kidney DPP-IV: elution profile on C4 RP-HPLC. RP-HPLC was performed on a C4 (7.5×200 mm) column with a linear gradient from 0 to 60% of solution B (acetonitrile in 0.1% of trifluoroacetic acid) for 60 min at a flow rate of 0.8 mL min^{-1}. The solid line indicates the absorbance at 215 nm, whereas the dashed line is the percentage of acetonitrile. Volume of loaded material was 100 μL. Several independent applications gave essentially the same chromatographic profiles.

Table 1. Effect of protease inhibitors and ions on rat kidney DPP-IV activity

Inhibitor	IC_{50}	K_i
TLCK	1.20±0.11 mM	nd
Bacitracin	0.32±0.01 mM	0.16±0.01 mM
Bestatin	0.45±0.06 mM	0.23±0.02 mM
L-Threo-Ile-thiazolidide	nd	64.00±0.53 nM
$CaCl_2$	38.05±1.54 mM	50.00± 1.05 mM*
$CoCl_2$	7.42±0.55 mM	nd
$CdCl_2$	3.87±0.22 mM	nd
$HgCl_2$	0.83±0.19 mM	nd
$ZnCl_2$	0.19±0.01 mM	0.15 ±0.01 mM*

Results are mean±SD (n=6); P32/98 K_i= 128.01±1.06 nM; nd: not determined; * K_i values correspond to the competitive component of the mixed inhibition.

the WHATIF program (Vriend 1990) to superpose porcine and rat DPP-IV and for root-mean-square deviation (RMSD) calculations.

2.7 *Data analysis*

Data represent the mean±SD values. ANOVA followed by Tukey–Kramer test was used to determine statistical significance between individual means. Differences were considered significant at $p<0.05$.

3. Results and discussion

3.1 *Purification of the intact membrane-bound form of rat kidney DPP-IV*

Rat kidney DPP-IV was isolated and purified to homogeneity by a combination of an extraction step, one clarification procedure and two chromatographic steps, as previously described for the porcine enzyme (Pascual *et al.* 2011). The treatment with 0.1% Triton X100 allowed the extraction of DPP-IV from membranes and the production of a highly enriched extract. The supernatant was treated at 60°C for 10 min, according to the temperature stability profiles of porcine (Pascual et al. 2011) and human DPP-IV. Despite

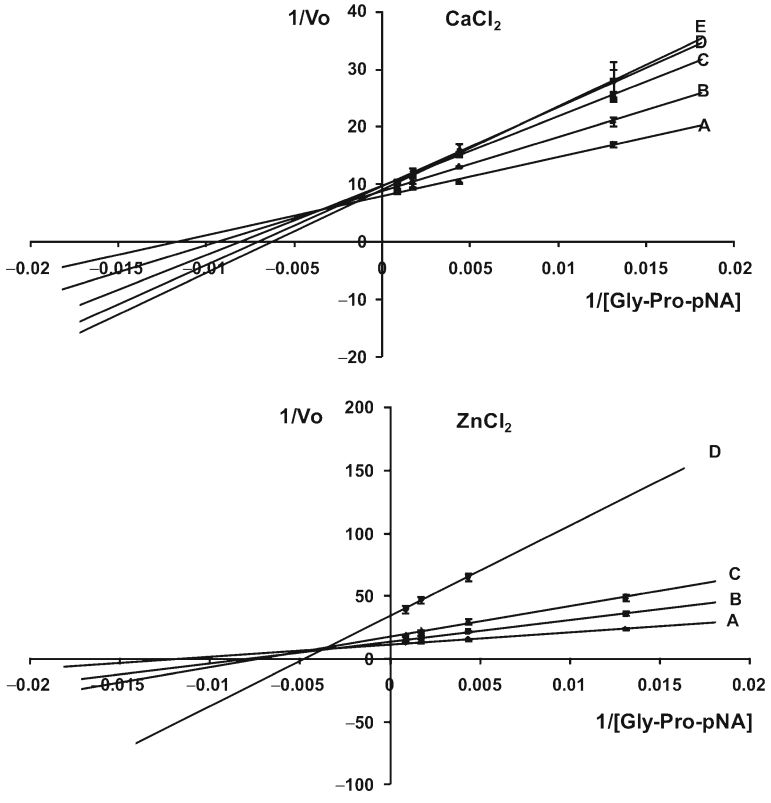

Figure 2. Establishment of the kinetic mechanism for rat kidney DPP-IV inhibition by calcium and zinc ions using Lineweaver–Burk plots. Letters A, B, C, D and E refer to the salt concentration in the assay, from the lowest to the highest. For Ca^{2+}, 0, 10, 50, 75 and 100 mM. For Zn^{2+}, 0, 0.1, 0.2 and 0.5 mM. Results are mean±SD (n=6).

Table 2. Ca^{2+} binding sites in rat and human DPP-IV predicted by GG, FEATURE and SeqFEATURE programs

Source	Site	Residues predicted by GG	Distance to active site (Å)	Score (/100)	
				FEATURE	SeqFEATURE
Human (recombinant)	1	$\mathbf{N}^{170}/\mathbf{D}^{171}/\mathbf{T}^{186}/\mathbf{N}^{196}$	30.94	8.39	17.30
	2	$\mathbf{S}^{158}/\mathbf{V}^{160}/\mathbf{G}^{161}$	37.44	-	12.66
	3	$\mathbf{D}^{243}{}_{A}/\mathbf{E}^{244}{}_{A}/\mathbf{L}^{246}{}_{A}/\mathbf{Y}^{661}{}_{B}$	18.37 (B) 28.30 (A)	2.60	3.96
	4	$\mathbf{Y}^{299}/\mathbf{R}^{318}/\mathbf{Q}^{320}/\mathbf{E}^{668}$	17.65	35.57	2.19
	5	$\mathbf{D}^{326}/\mathbf{C}^{339}/\mathbf{L}^{340}/\mathbf{Q}^{344}$	37.26	9.02	3.98
	6	$\mathbf{E}^{205}/\mathbf{E}^{206}/\mathbf{Y}^{662}$	6.58	5.83	16.77
	7	$\mathbf{Y}^{128}/\mathbf{Y}^{132}/\mathbf{T}^{152}/\mathbf{Q}^{153}$	25.13	32.44	-
	8	$\mathbf{D}^{104}/\mathbf{E}^{117}/\mathbf{Y}^{128}$	23.63	19.33	2.45
Rat (kidney)	1	$\mathbf{E}^{71}/\mathbf{N}^{90}/\mathbf{NAG}^{1090}$	38.25	2.38	19.49
	2	$\mathbf{Y}^{239}{}_{A}/\mathbf{S}^{240}{}_{A}/\mathbf{D}^{241}{}_{A}/\mathbf{Q}^{719}{}_{A}$	19.47 (B) 26.31 (A)	24.28	10.25
	3	$\mathbf{E}^{235}{}_{A}/\mathbf{E}^{235}{}_{B}/\mathbf{S}^{237}{}_{B}$	21.05 (A) 21.54 (B)	22.01	11.84
	4	$\mathbf{L}^{76}/\mathbf{N}^{83}/\mathbf{S}^{84}/\mathbf{NAG}^{1083}$	43.36	-	28.05
	5	$\mathbf{E}^{235}{}_{A}/\mathbf{P}^{247}{}_{B}/\mathbf{K}^{248}{}_{B}/\mathbf{T}^{249}{}_{B}$	20.45 (A) 25.16 (B)	3.65	15.94
	6	$\mathbf{D}^{102}/\mathbf{E}^{115}/\mathbf{Y}^{126}$	24.58	4.23	13.53
	7	$\mathbf{N}^{431}/\mathbf{S}^{447}/\mathbf{C}^{448}/\mathbf{C}^{455}$	31.15	-	6.57
	8	$\mathbf{Y}^{126}/\mathbf{Y}^{130}/\mathbf{T}^{150}/\mathbf{Q}^{151}$	25.02	0.73	16.06
	9	$\mathbf{N}^{227}/\mathbf{T}^{263}/\mathbf{NAG}^{1227}$	26.70	2.79	2.33

We specify in each case the residues implicated in ion coordination, and the distance of the residue to the DPP-IV active site, taking as reference point the hydroxyl group of S630. A: monomer A; B: monomer B. The distance to the active site refers to monomer A active site, except for the binding sites located at the interface of both monomers. In the latest case the distance to each active site is depicted.

reduced heat stability for rat DPP-IV compared to that of the porcine and human homologs, this step allowed the elimination of a large number of protein contaminants; the extract had an enzyme-specific activity of 1.57×10^{-5} U/mg. On DEAE-Sephacel chromatography, DPP-IV activity eluted at 0.15 M NaCl. This chromatography produced a significant removal of contaminant proteins and increased the enzyme purity (enzyme-specific activity of 27.1×10^{-5} U/mg). In Sephadex G-200 chromatography, DPP-IV activity eluted after the void volume of the column in a position corresponding to a molecular weight around 260 kDa, indicating the presence of a dimeric form of the enzyme (not shown). This step increased enzyme purity (enzyme-specific activity of 55.0×10^{-5} U/mg), with an adequate overall yield of the procedure (purification fold of 36.4 times, 36.5% of enzyme activity recovery). The purity of the enzyme was corroborated by the presence of a single, stretched and symmetrical peak in a RP-HPLC C4 chromatography (figure 1). The purified preparation was devoid of aminopeptidase contaminants, as demonstrated by the absence of hydrolysis of the specific substrates for APN, APA or APB (not shown).

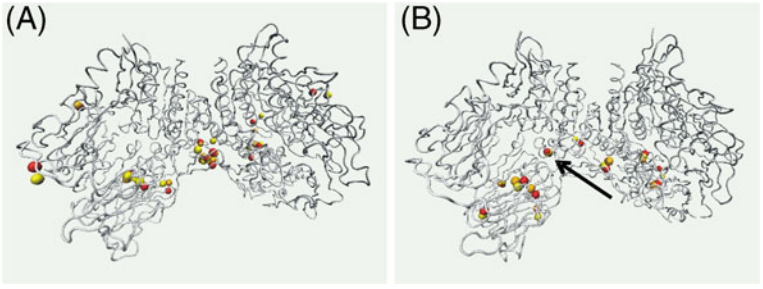

Figure 3. Predicted Ca^{2+} binding sites in dimeric rat and human DPP-IV. Location of Ca^{2+} binding sites in rat (**A**) and human (**B**) DPP-IV, as predicted using GG, FEATURE and SeqFEATURE programs (calcium represented as red, orange and yellow spheres, respectively). The black arrow indicates the Ca^{2+} coordination residues located at the human DPP-IV active site, absent in rat DPP-IV. Figures were generated with VMD.

Table 3. Distance between residues and values of the dihedral angles for the residues E^{205}, E^{206} and Y^{662} of the porcine DPP-IV, or for equivalent residues of the human and rat DPP-IV

Source	Residue	Distance (Å)* Y^{662}	Dihedral angles		
			χ_1	χ_2	χ_3
Porcine (kidney)	**E^{205}**	4.8	169.9	72.6	10.3
	E^{206}	3.5	−47.8	−66.4	2.0
	Y^{662}	-	-155.1	51.0	-
Human (recombinant)	**E^{205}**	5.3	176.9	59.5	30.6
	E^{206}	3.6	−52.0	−75.2	34.3
	Y^{662}	-	−155.4	47.2	-
		Y^{663}			
Rat (kidney)	**E^{203}**	4.4	−179.7	61.6	24.8
	E_{204}	3.2	−52.5	−58.3	−13.3
	Y^{663}	-	−153.2	50.2	-

*The distance between the OD2 atom of the Glu residues and the OH group of Tyr was calculated.

3.2 *Kinetic characterization of rat kidney DPP-IV*

The pH-activity profile indicated an optimum pH value for the purified rat kidney DPP-IV around 8.0, and a strong reduction of enzyme activity above pH 9 and below pH 6 (not shown); these data were similar to those data reported for the porcine enzyme (Pascual *et al.* 2011), and for DPP-IV from other sources (Wolf *et al.* 1989; Leiting *et al.* 2003). Gly-Pro-pNA was hydrolysed with a V_{max} of 0.86±0.01 μmol $min^{-1}mL^{-1}$ and K_M of 76±6 μM; these values are in the same order of magnitude as those previously reported for DPP-IV from different mammalian sources (Wolf *et al.* 1989; Pascual *et al.* 2011).

3.3 *Effect of inhibitors on rat kidney DPP-IV*

Purified rat kidney DPP-IV was irreversibly inhibited by TLCK, and reversibly inhibited in a competitive way by bacitracin and bestatin, a metallo aminopeptidase inhibitor. P32/98, a specific inhibitor for the DPP-IV family, inhibited rat DPP-IV through a tight binding mechanism (table 1). These data are consistent with the previously established susceptibility of DPP-IV to low-molecular-weight inhibitors (Svensson *et al.* 1978; Wolf *et al.* 1989; Thornberry and Gallwitz 2009; Pascual *et al.* 2011). The enzyme was not sensitive to chelating agents (0.1–5.0 mM of EDTA or EGTA, or 1 mM 1,10-phenanthroline) or to 0.1–10 mM NEM (not shown). Since NEM alkylates cystein residues and non-competitively inhibits DPP-8 and DPP-9 (in the classical sense) but not DPP-IV, its lack of effect indicates that the preparation was devoid of DPP-8 and DPP-9 (Park *et al.* 2008; Yu *et al.* 2010), and that the enzymatic properties should only be ascribed to DPP-IV.

3.4 *Effect of divalent ions on rat kidney DPP-IV and prediction of Ca^{2+} and Zn^{2+} binding sites in rat and human DPP-IV structures using bioinformatic tools*

Among the ions tested, only Cd^{2+}, Hg^{2+}, Ca^{2+}, Co^{2+} and Zn^{2+} significantly reduced the enzyme activity. For these

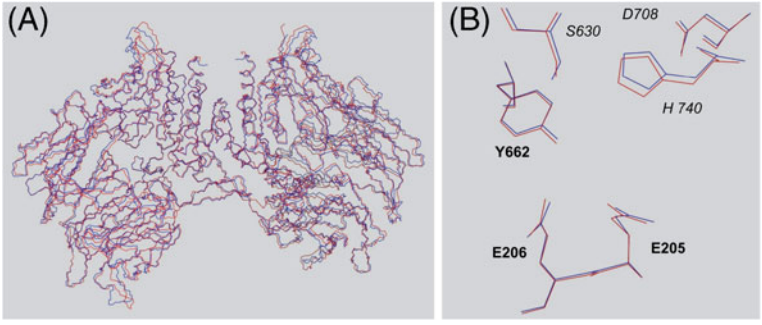

Figure 4. Superposition of porcine and rat DPP-IV structures. (**A**) Superposition of the backbone of porcine (red) and rat (blue) DPP-IV enzymes. (**B**) Superposition of the residues implicated in Ca^{2+} coordination (bold letters) and the catalytic triad (italic letters). Figures were generated with CHIMERA.

Table 4. Residues of rat and human DPP-IV predicted to coordinate Zn^{2+} according to the MetSite program

Source	Residues with potentialities to coordinate Zn^{2+}	Distance to active site (Å)	Score (/1)
Human (recombinant)	H^{740}	2.94	0.75
	D^{708}	7.07	0.36
	G^{741}	9.81	0.61
	G^{705}	12.43	0.43
	C^{551}	12.97	0.39
	C^{649}	20.86	0.36
	C^{762}	22.80	0.60
	E^{699}	24.98	0.69
	E^{67}	42.89	0.34
Rat (kidney)	H^{741}	3.31	0.66
	D^{709}	7.35	0.63
	G^{550}	8.56	0.58
	H^{713}	12.03	0.41
	E^{404}	21.44	0.56
	G^{477}	28.11	0.36
	D^{169}	32.40	0.42

The residues with a score higher that 0.2 are included. Data for a catalytic triad residue are in bold. The distance to active site refers to monomer A active site.

ions a wide range of IC_{50} values was observed (table 1). These values are of the same or similar order of magnitude as for the porcine enzyme (Pascual *et al.* 2011) indicating a similar susceptibility.

For zinc and calcium ions, we observed kinetic mechanisms of linear mixed inhibition (figure 2), as previously reported for the porcine enzyme with effects on K_M and V_{max} (Pascual *et al.* 2011); the K_i values of the competitive components are listed on table 1. Similarly to the porcine DPP-IV, K_i values for the rat enzyme were lower for zinc than for calcium (table 1), but the values differed among species; the porcine enzyme was more strongly inhibited by Zn^{2+} than the rat enzyme, while the reverse was observed for Ca^{2+}. Calcium plasma concentrations are tightly regulated and range from 2.2 to 2.6 mM, although its ionic form determines the physiologic effect of this element, with plasma concentration in the 1.1–1.4 mM range. IC_{50} values for the human enzyme are just above the normal plasma levels (Wolf *et al.* 1989); therefore, we cannot discard a regulatory effect of this ion on DPP-IV activity in human and rat enzymes. The susceptibility of DPP-IV activity from different sources (mammals and microorganisms) to the presence of divalent ions such as Zn^{2+} and Ca^{2+} has been previously reported (Wolf *et al.* 1989; Mantle 1991; Koreeda *et al* 2001). Moreover, we have recently reported that for the porcine DPP-IV these ions act through a kinetic mechanism of mixed inhibition (Pascual *et al.* 2011). These kinetic data were corroborated in the present work for the rat homolog. This type of inhibition indicates both an effect on the recognition of the substrate by the enzyme and on the catalytic degradation.

The results for the prediction of Ca^{2+} binding sites in the rat and human DPP-IV are summarized in table 2. For the rat enzyme, all sites predicted are formed by amino acids located at the β-propeller domain (figure 3A). There was a difference with the sites predicted for the human enzyme, which included a binding position in the vicinity of the catalytic residue S^{630} (at 6.27 Å and 6.58 Å for the monomers A and B, respectively) (figure 3B), as previously reported for the porcine homolog (Pascual *et al.* 2011). The structure of this binding site in the porcine enzyme includes E^{205}, E^{206} and Y^{662}, residues involved in substrate recognition and fixation via electrostatic interactions with the amino terminus of the substrate. In this regard we calculated the distances between residues and dihedral angles of residues implicated in the binding sites previously described for the porcine enzyme (table 3), using the program WATHIF. The distance between glutamic acid and tyrosine residues was smaller for rat DPP-IV than for the porcine and human homologs. In addition, the dihedral angle χ_1 of the residue E^{205} in porcine and human DPP-IV was 169.9° and 176.9°, respectively, whereas it was −179.7° for the equivalent E^{203} in rat DPP-IV. This difference could explain the improper orientation of these residues oxygen atoms, compared to those that presumably coordinate Ca^{2+} in the porcine DPP-

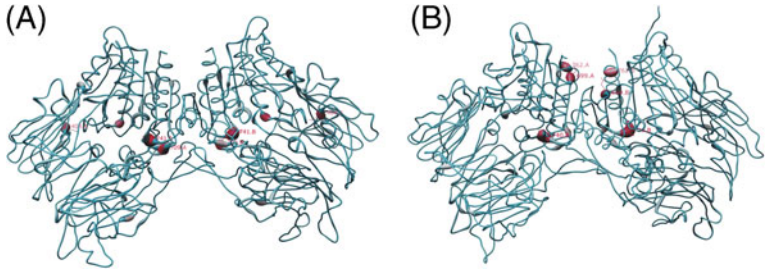

Figure 5. Predicted Zn^{2+} binding sites in dimeric rat and human DPP-IV. Location of Zn^{2+} binding sites in rat (**A**) and human (**B**) DPP-IV, as predicted with the MetSite program; the ellipsoids represent zinc. The figure was generated with CHIMERA.

IV. It should be pointed out that the predictions were performed from only one structure (PDB 2gbc for rat DPP-IV), and therefore we cannot rule out definitively the occurrence of a Ca^{2+} binding site in that position in rat DPP-IV. Some of the programs used (i.e. GG) are quite sensitive to the geometrical orientation of the putative coordinating atoms; since protein structures are intrinsically dynamic, it remains possible that residues E^{203}, E^{204} and Y^{663} could bind Ca^{2+}. This possibility is consistent with the fact that an overall high structural similitude exits between porcine and rat DPP-IV (RMSD=0.681 Å) (figure 4).

The prediction of Zn^{2+} binding sites for the rat and human DPP-IV was performed with the MetSite program and the results are summarized in table 4. This program evaluates the potentiality of each individual residue in the protein to coordinate one Zn^{2+} ion and scores it in the range 0–1. For both rat and human DPP-IV at least one of the members of the catalytic triad was predicted to coordinate Zn^{2+}. Moreover, all the predicted residues with a score higher than 0.2 were positioned in the catalytic domain (α-β hydrolase domain) (figure 5). This result is similar to that previously described for porcine DPP-IV (Pascual *et al.* 2011) and may explain the intense inhibitory effect of Zn^{2+} on the enzyme activity with changes in K_M and k_{cat}. Thus, zinc susceptibility is probably a general property of DPP-IV from distinct mammalian sources; this property may be useful in glucose metabolism control (Jansen *et al.* 2009). In particular, the confirmation in rat and human of the prediction that the catalytic histidine residue binds Zn^{2+} (Pascual *et al.* 2011) supports the proposal for the rational design of DPP-IV inhibitors that combine Zn^{2+} coordination groups with DPP-IV specificity moieties. This feature would presumably improve their potency as therapeutic agents not only in the treatment of type 2 diabetes mellitus, but also in other pathologies involving increased DPP-IV activity (Bank *et al.* 2008; Yu *et al.* 2010) and zinc deficiency (Jansen *et al.* 2009). The supplementation of zinc in different coordination environments lowers serum glucose concentration and offers additional beneficial effects for the therapeutic management of diabetes type 2 (Yoshikawa *et al.* 2011; Jayawardena *et al.* 2012); therefore, the proposed strategy for the development of new potent and specific DPP-IV inhibitors may lead to promising biomedical applications.

4. Conclusions

We have purified rat kidney DPP-IV to homogeneity. The kinetic behaviour of the enzyme and its sensitivity to inhibitors were consistent with the known properties for other mammalian DPP-IV homologs. Rat DPP-IV was inhibited by calcium and zinc ions through a mixed mechanism. K_i values indicated some differences between mammalian orthologues. Moreover, in rat and human DPP-IV, predicted Ca^{2+} and Zn^{2+} binding sites were located in the β-propeller and α-β hydrolase domains, respectively. Some other major aspects were also conserved, such as a significant degree of inhibition by zinc. This susceptibility may be relevant for the molecular basis of pathologies involving an imbalance of levels of Zn^{2+} ions, and may be of use to develop better drugs for pathologies in which DPP-IV activity is involved.

Acknowledgements

This work was funded by grants from the International Foundation for Science (IFS) and the Organization for the Prohibition of Chemical Weapons (OPCW) (F/3276-3), CONACYT-Mexico (61804), CONACYT-Mexico-Cuba-CITMA (2009-2011), and OPCW Internship 2010 to IP.

References

Bank U, Bohr UR, Reinhold D, Lendeckel U, Ansorge S, Malfertheiner P and Tager M 2008 Inflammatory bowel diseases: multiple benefits from therapy with dipeptidyl- and alanyl-aminopeptidase inhibitors. *Front. Biosci.* **13** 3699–3713

Chávez MA, Díaz J, Delfín J and Pérez U 1990 *Temas de Enzimología. Tomo I. La Habana* (Empresa Nacional de Publicaciones de la Educación Superior)

Copeland R 2000 *Enzymes, A practical introduction to structure, mechanism, and data analysis* (Wiley-VCH Inc)

Cornish-Bowden A 2012 *Fundamentals of enzyme kinetics* (Germany: Wiley-Blackwell)

Deng H, Chen G, Yang W and Yang JJ 2006 Predicting calcium-binding sites in proteins - A graph theory and geometry approach. *Proteins* **64** 34–42

Gorrell MD 2005 Dipeptidyl peptidase IV and related enzymes in cell biology and liver disorders. *Clin. Sci.* **108** 1–16

Humphrey W, Dalke A and Schulten K 1996 VMD - Visual molecular dynamics. *J. Mol. Graph.* **14** 33–38

Jansen J, Karges W and Rink 2009 Zinc and diabetes–clinical links and molecular mechanisms. *J. Nutr. Biochem.* **20** 399–417

Jayawardena R, Ranasinghe P, Galappatthy P, Malkanthi RL, Constantine G and Katulanda P 2012 Effects of zinc supplementation on diabetes mellitus: a systematic review and meta-analysis. *Diabetol. Metab. Syndr.* doi:10.1186/1758-5996-4-13

Koreeda Y, Hayakawa M, Ikemi T and Abiko Y 2001 Isolation and characterisation of dipeptidyl peptidase IV from *Prevotella loescheii* ATCC 15930. *Arch. Oral. Biol.* **46** 759–766

Lankas G, Leiting B, Roy R, Eiermann G, Beconi M, Biftu T, Chan Ch, Edmondson S, *et al.* 2005 Dipeptidyl peptidase IV inhibition for the treatment of type 2 diabetes. Potential importance of selectivity over dipeptidyl peptidases 8 and 9. *Diabetes* **54** 2988–2994

Leatherbarrow RJ 1993 GRAFIT: Data analysis and graphics program. Version 3.01 (Erithacus Software Ltd)

Leiting B, Pryor KD, Wu JK, Marsilio F, Patel RA, Craik ChS, Ellmanœ JA, Cummings RT and Thornberry NA 2003 Catalytic

properties and inhibition of proline-specific dipeptidyl peptidases II, IV and VII. *Biochem. J.* **371** 525–532

Liang MP, Banatao DR, Klein TE, Brutlag DL and Altman RB 2003 WebFEATURE: an interactive Web tool for identifying and visualizing functional sites on macromolecular structures. *Nucleic Acids Res.* **31** 3324–3327

Longenecker KL, Stewart KD, Madar DJ, Jakob CG, Fry EH, Wilk S, Lin CW, Ballaron SJ, *et al*. 2006 Crystal structures of DPP-IV (CD26) from rat kidney exhibit flexible accommodation of peptidase-selective inhibitors. *Biochemistry* **45** 7474–7482

Mantle D 1991 Characterization of dipeptidyl and tripeptidyl aminopeptidases in human kidney soluble fraction. *Clin. Chim. Acta.* **196** 135–142

Matteucci E and Giampietro O 2009 Dipeptidyl peptidase-4 (CD26): knowing the function before inhibiting the enzyme. *Curr. Med. Chem.* **16** 2943–2951

Nagatsu T, Hino M, Fuyamada H, Hayakawa T and Sakakibara S 1976 New chromogenic substrates for X-prolyl dipeptidyl-aminopeptidase. *Anal. Biochem.* **74** 466–476

Oefner C, D'Arcy A, Mac Sweeney A, Pierau S, Gardiner R and Dale GE 2003 High-resolution structure of human apo dipeptidyl peptidase IV/CD26 and its complex with 1-[([2-[(5-iodopyridin-2-yl)amino]-ethyl]amino)-acetyl]-2-cyano-(S)-pyrrolidine. *Acta Crystallogr. D Biol. Crystallogr*. **59** 1206–1212

Park J, Knott HM, Nadvi NA, Collyer CA, Wang XM, Church WB and Gorrell MD 2008 Reversible inactivation of human dipeptidyl peptidases 8 and 9 by oxidation. *Open Enz. Inhibit. J.* **1** 52–61

Pascual I, Gómez H, Pons T, Chappé M, Vargas MA, Valdés G, Lopéz A, Saroyán A, Charli JL and Chávez MA 2011 Effect of divalent cations on the porcine kidney cortex membrane-bound form of dipeptidyl peptidase IV. *Int. J. Biochem. Cell Biol.* **43** 363–371

Peters A 2010 Incretin-based therapies: review of current clinical trial data. *Am. J. Med.* **123** 28–37

Pettersen EF, Goddard TD, Huang CC, Couch GS, Greenblatt DM, Meng EC and Ferrin TE 2004 UCSF CHIMERA - A visualization system for exploratory research and analysis. *J. Comput. Chem.* **25** 1605–1612

Scopes R. 1987 *Protein purification: principles and practice* (Springler-Verlag)

Sodhi JS, Bryson K, McGuffin LJ, Ward JJ, Wernisch L and Jones DT 2004 Predicting metal-binding site residues in low-resolution structural models. *J. Mol. Biol.* **342** 307–320

Stulc T and Sedo A 2010 Inhibition of multifunctional dipeptidyl peptidase-IV: Is there a risk of oncological and immunological adverse effects? *Diabetes Res. Clin. Pract.* **88** 125–131

Svensson B, Danielsen M, Staun M, Jeppesen L, Norén O and Sjöström H 1978 An amphiphilic form of dipeptidyl peptidase IV from the pig small-intestinal brush-border membrane. Purification by immunoadsorbent chromatography and some properties. *Eur. J. Biochem.* **90** 489–498

Thornberry NA and Gallwitz B 2009 Mechanism of action of inhibitors of dipeptidyl-peptidase-4 (DPP-4). *Best Pract. Res. Clin. Endocrinol. Metab*. **23** 479–486

Tieku T and Hooper M 1992 Inhibition of aminopeptidases N, A and W: a re-evaluation of the actions of bestatin and inhibitors of angiotensin converting enzyme. *Biochem. Pharmacol.* **44** 1725–1730

Vriend G 1990 WHATIF, a molecular modeling and drug design program. *J. Mol. Graph*. **8** 52–56

Wilson MJ, Haller R, Li SY, Slaton JW, Sinha AA and Wasserman NF 2005 Elevation of dipeptidylpeptidase iv activities in the prostate peripheral zone and prostatic secretions of men with prostate cancer: possible prostate cancer disease marker. *J. Urol.* **174** 1124–1128

Wolf GB, Scherberich GB, Foscher P and Scharpe W 1989 Isolation and characterization of dipeptidyl aminopeptidase IV from human kidney cortex. *Clin. Chim. Acta.* **179** 61–72

Yazbeck R, Howarth GS, Abbott CA 2009 Dipeptidyl peptidase inhibitors, an emerging drug class for inflammatory disease? *Trends Pharmacol. Sci.* **30** 600–607

Yilmaz Y, Atug O, Yonal O, Duman D, Ozdogan O, Imeryuz N and Kalayci C 2009 Dipeptidyl peptidase IV inhibitors: therapeutic potential in nonalcoholic fatty liver disease. *Med. Sci. Monit.* **15** 1–5

Yoshikawa Y, Adachi Y, Yasui H, Hattori M and Sakurai H 2011 Oral administration of bis(aspirinato)zinc(II) complex ameliorates hyperglycemia and metabolic syndrome-Like disorders in spontaneously diabetic KK-Ay mice: structure–activity relationship on zinc–salicylate complexes. *Chem. Pharm. Bull.* **59** 972–977

Yu D, Yao TW, Chowdhury S, Nadvi NA, Osborne B, Church WB, McCaughan GW and Gorrell M 2010 The dipeptidyl peptidase IV family in cancer and cell biology. *FEBS J.* **277** 1126–1144

MS received 16 January 2013; accepted 08 April 2013

Corresponding editor: María Luz Cárdenas